THE ASTROPHYSICAL JOURNAL, 388:400–414, 1992 April 1

THE STAR FORMATION HISTORY OF THE LARGE MAGELLANIC CLOUD

GIANPAOLO BERTELLI,[1,2] MARIO MATEO,[3,4] CESARE CHIOSI,[2] AND ALESSANDRO BRESSAN[5]
Received 1991 May 9; accepted 1991 October 8

ABSTRACT

We present deep photometric observations of stars in three fields of the Large Magellanic Cloud (LMC) and interpret these data using synthetic color-magnitude diagrams (CMDs) and luminosity functions (LFs) generated from the overshoot models of Bertelli et al., Bressan et al., and Aparicio et al. We can successfully model the field CMDs *and* LFs with a star formation rate that experienced a large increase $(4 \pm 0.5) \times 10^9$ yr ago. The precise age of this "burst" depends sensitively on the characteristics of the models. Classical (i.e., nonovershoot) models yield a burst age about 2×10^9 yr younger than the value we obtain. An initial mass function with slope of 2.35 (the Salpeter value) and a mean field star metallicity of [Fe/H] ~ -0.7 are consistent with the photometric data and LFs. Furthermore, our primary conclusion, that is, the possibility of a single burst of star formation, depends on the distance modulus adopted for LMC. If $(m - M)_0 = 18.4$, we find evidence for a single burst throughout the LMC. If $(m - M)_0 = 18.6$, this is no longer possible. Given the differences between the ages derived using overshoot and classical models, the age distribution we derive for LMC field stars older than about 1×10^9 yr is similar to that found by earlier studies using deep photographic observations of other fields throughout the LMC, and with the observed age distribution of intermediate-age and old LMC star clusters. This suggests that the star formation rate in the LMC was globally quite low during at least the first half of its lifetime, and that a major event triggered a substantial and relatively sudden increase in the star formation rate throughout the entire LMC which persisted for several 10^9 yr and even up to the present epoch in some parts of that galaxy.

Subject headings: galaxies: stellar content — Magellanic Clouds — stars: evolution — stars: formation

1. INTRODUCTION

A growing body of evidence suggests that the Large Magellanic Cloud (LMC) has experienced significant variations in its star formation rate (SFR). Tifft & Snell (1971) and Hodge (1973) noted that the LMC has contained a number of distinct active star-forming regions over the past $\sim 10^8$ yr. Today we see one such active region around 30 Dor, whereas the Constellation III region (van den Bergh 1984; Nail & Shapley 1953) represents a similar, but older, region of enhanced star formation. These conclusions were based on the distribution and photometric properties of young bright stars, blue clusters, and associations in various parts of the LMC. Butcher (1977) first undertook the more difficult task of ascertaining the star formation history of the LMC at even greater ages by identifying the observed break in the field-star luminosity function at $M_V \sim +3.5$ with star clusters possessing main-sequence turnoffs at this same luminosity. In this way, Butcher concluded that the LMC appears to have formed the bulk of its stars at some intermediate epoch about $(3–4) \times 10^9$ yr ago. Subsequent studies using similar techniques (Stryker 1984) have confirmed this general result. All of this work, however, was based on analyses at the very limits of reliability of photographic photometry. Independent verification of Butcher's findings was provided by the work of Frogel & Blanco (1983) and Hardy et al. (1984) who argued for the existence of a "strong" intermediate-age component in two regions near the center of the LMC on the basis of the observed distribution of evolved luminous giants and sub–giant branch stars, respectively. Star clusters may also be used to estimate the star formation history of the LMC. In agreement with the field star work, recent studies using only clusters with precisely determined ages (Mateo 1988a; Olszewski et al. 1991; Da Costa 1991) agree that the LMC contains virtually no clusters older than about $(3–4) \times 10^9$ yr, except for a small population of ancient $(12–15) \times 10^9$ yr old systems.

In this paper we present an analysis of deep CCD observations in three fields located more than 4° (about 3.5 kpc) from the center of the LMC and address the following issues. First, when did the apparent enhancement in the LMC field star formation rate commence, and how long did it continue after it began? Second, did this star formation event involve the entire LMC, or is there evidence that different fields have experienced significantly different star formation histories? Our approach in this study is to use stellar evolutionary models of Bertelli et al. (1985, 1986a, b, 1990) and Bressan, Bertelli, & Chiosi (1986) to quantitatively constrain the *form* of the star formation history in the observed LMC fields, and to provide a precise estimate of the age of the intermediate-age stellar component that appears to comprise a large fraction of the population of LMC field stars. To this end, we have parameterized plausible star formation histories for the LMC, and we discuss briefly the constraints that our observations place on these scenarios.

Section 2 presents the observations, the data reduction, and the completeness analysis. Section 3 deals with the theoretical analysis of suitable field star counts used to infer the star formation rate. The comparison of theoretical models with observations and determination of the age dependence of the star

[1] Fellow of the National Council of Research, CNR-GNA, Rome, Italy.
[2] Department of Astronomy, University of Padua, Vicolo Osservatorio 5, 35122 Padova, Italy.
[3] The Observatories of the Carnegie Institution of Washington, 813 Santa Barbara Street, Pasadena, CA 91101.
[4] Hubble Fellow. Visiting Astronomer at the Cerro Tololo Inter-American Observatory, National Optical Astronomy Observatory, operated by the Association of Universities for Research in Astronomy, Inc., under contract with the National Science Foundation.
[5] Astronomical Observatory, Vicolo Osservatorio 5, 35122 Padova, Italy.

TABLE 1

SUMMARY OF OBSERVATIONS OF LMC FIELDS

Field	α	δ	R_{LMC}	Exposure Time: B^a	Exposure Time: V^a	N_{CMD}
NGC 1783.....	$04^h58^m8^s$	$-66°02'$	4°.5	240; 3600	200; 3000	2028
NGC 1866.....	05 13 4	−65 29	4.4	200; 3000	160; 2700	2372
NGC 2155.....	05 58 3	−65 28	5.5	100; 1000	50; 1000	1779

[a] Exposure times are in seconds.

formation law are given in § 4. Finally, some concluding remarks are presented in § 5.

2. OBSERVATIONS AND REDUCTIONS

The data used in this study were obtained with the prime-focus RCA CCD camera at the CTIO 4 m telescope during two separate observing runs. The *BV* CCD frames discussed here were taken as control regions for the three LMC clusters NGC 1783, NGC 1866, and NGC 2155. Local standards in the NGC 1783 and NGC 1866 fields used in this study were established during an excellent photometric run at the CTIO 0.9 m immediately before the 4 m run. These 0.9 m observations were in turn calibrated via direct observations of numerous (≥ 20) *BV* *E*-region standards; the standard deviation of the standard star photometry about the adopted *BV* transformations was less than 0.02 mag for all the 0.9 m nights (Mateo, Olszewski, & Madore 1990). The NGC 2155 photometry was directly calibrated via observations of Graham (1981, 1982) standards obtained with the 4 m telescope. The standard deviation of the standards about the adopted *BV* transformations was ≤ 0.02 mag (Olszewski, Schommer, & Aaronson 1987). Combined with the uncertainties in the aperture corrections for the program CCD images, we estimate that the systematic errors in V and $(B-V)$ for each field are about 0.02–0.03 mag. Although the fields used in this study are all located relatively near populous clusters, the contamination by cluster stars is nevertheless probably very slight. For example, in the case of NGC 1866, Elson, Fall, & Freeman (1987) and Fischer et al. (1991) present surface brightness profiles that show the cluster contributes less than 1% to the field star counts in the field used in this study ($R > 90$ pc). For the NGC 1783 and NGC 2155 fields, the contamination will be even less because (1) the clusters are smaller (Mateo 1987a) and (2) in the case of NGC 2155 the field is located even further from the cluster center.

Each CCD frame used in this study covers about 15 arcmin^2. Table 1 lists some of the properties of the observational data and the LMC fields. In particular, N_{CMD} is the total number of stars measured in each field, whereas R_{LMC} is the distance from the LMC center. The exposure times are in seconds. The CCD frames were reduced using the two-dimensional photometry program DoPHOT (Mateo & Schechter 1989).

The observational color-magnitude diagrams (CMD) are shown in the left panels of Figures 1–3 for the NGC 1783, NGC 1866, and NGC 2155 fields, respectively. The total numbers of stars in the three CMDs are listed in Table 1, whereas star counts per magnitude bin in selected areas of the CMD are given in Table 2.

The observational luminosity functions (LFs) (before applying the correction for photometric incompleteness) are given as the cumulative number of stars with apparent magnitude $V \leq V_{MAX}$ and separately for main-sequence and post–main-sequence stars. The distinction between the two groups is

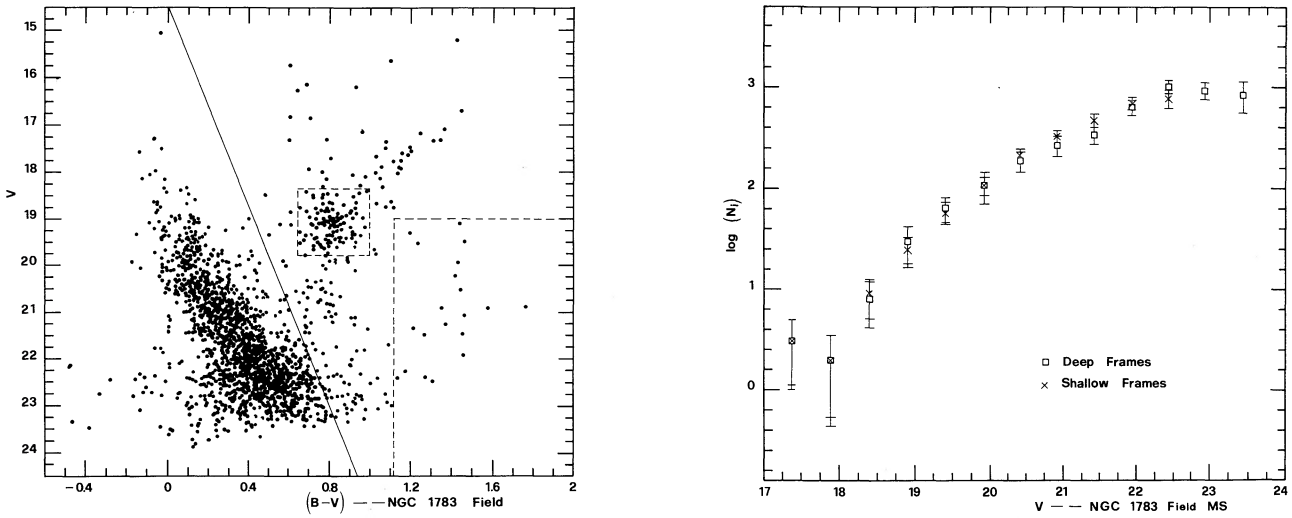

FIG. 1.—Color magnitude diagram (*left*) and differential luminosity functions (*right*) for the field near NGC 1783. The diagonal line in the left panel denotes the demarcation line between the "blue" and "red" stars (physically between main-sequence and post–main-sequence stars). The large dashed rectangle encloses stars that are likely foreground objects according to the predicted counts by Ratnatunga & Bahcall (1985). The small dashed rectangle encloses stars in the red clump (likely core He-burners). The total number of these is $N_{RC} = 118$. Note the good agreement between the luminosity functions determined on the short- and long-exposure *BV* CCD frames pairs.

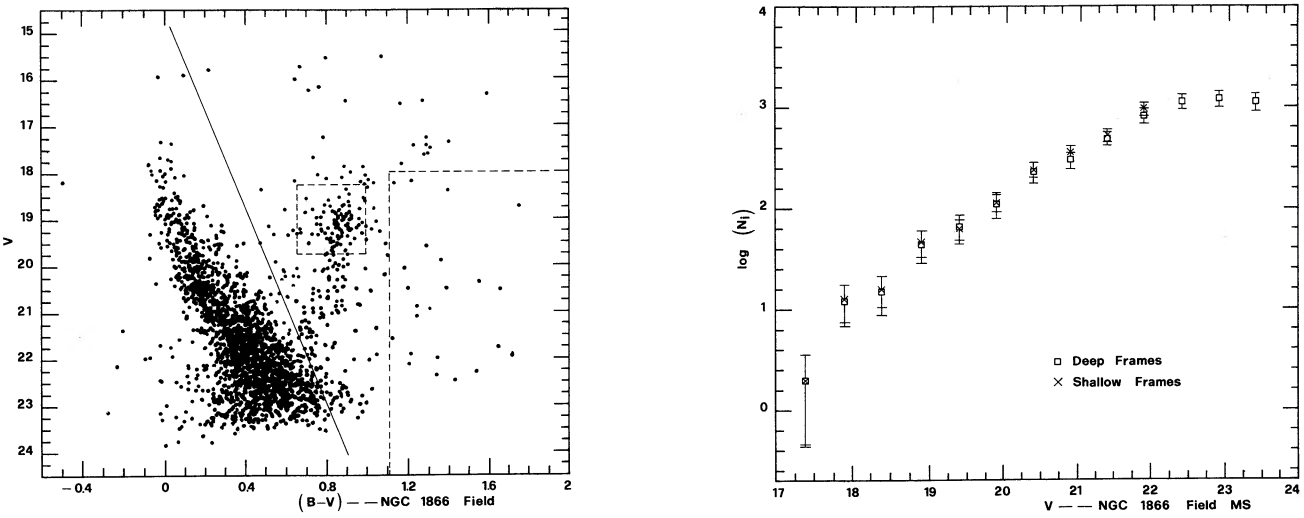

FIG. 2.—Same as in Fig. 1 but for the field near NGC 1866. Total number of stars in the red clump box is $N_{RC} = 97$.

based on the eye-drawn line shown in the CMDs of Figures 1–3 (left panels). The star counts are presented in Table 2, where N, N_B, and N_R stand for the cumulative number of all stars, main-sequence, and post–main-sequence objects, respectively. For each field, we also give in Table 2 the number N_{RC} of stars falling in the box centered on the red clump as shown in Figures 1–3. It is worth noticing that although the entries in Table 2 span the magnitude range down to $V = 25$, our analysis will be limited to stars brighter than $V = 22.5$ for which the correction for photometric completeness is small (see below).

The completeness corrections to be applied to the observational LFs were determined as a function of magnitude and color via false-star experiments similar to those described by Mateo (1988b) and Stetson & Harris (1988). Twenty-four such experiments were carried out in each field for each color (i.e., 48 per field). The completeness corrections reach a factor of three at $V \sim 23$ for each field. The results of the completeness analysis are given in Table 3 for the B and V passbands. In practice, only magnitude bins where the completeness corrections are at least 0.4–0.5 or larger have been used in the analysis. The corrected luminosity functions are shown in the right panels of Figures 1, 2, and 3 for the NGC 1783, NGC 1866, and NGC 2155 fields, respectively. The excellent agreement between the field LFs derived from the short- and long-exposure frame pairs suggests that the completeness corrections have been well-determined and consistently applied to the observed LFs.

A well-defined main sequence of LMC field stars is clearly observed in the CMD of each field, as are a large number of red giants and red clump stars at $(B-V) \sim 0.9$ and $V \sim 19$. There are also important differences in the morphologies of the CMDs of the three fields; for example, the shapes of the red clumps and the maximum luminosity attained by main-sequence stars differ significantly in the fields. The stars located within the large dashed rectangles in Figures 1–3 are likely

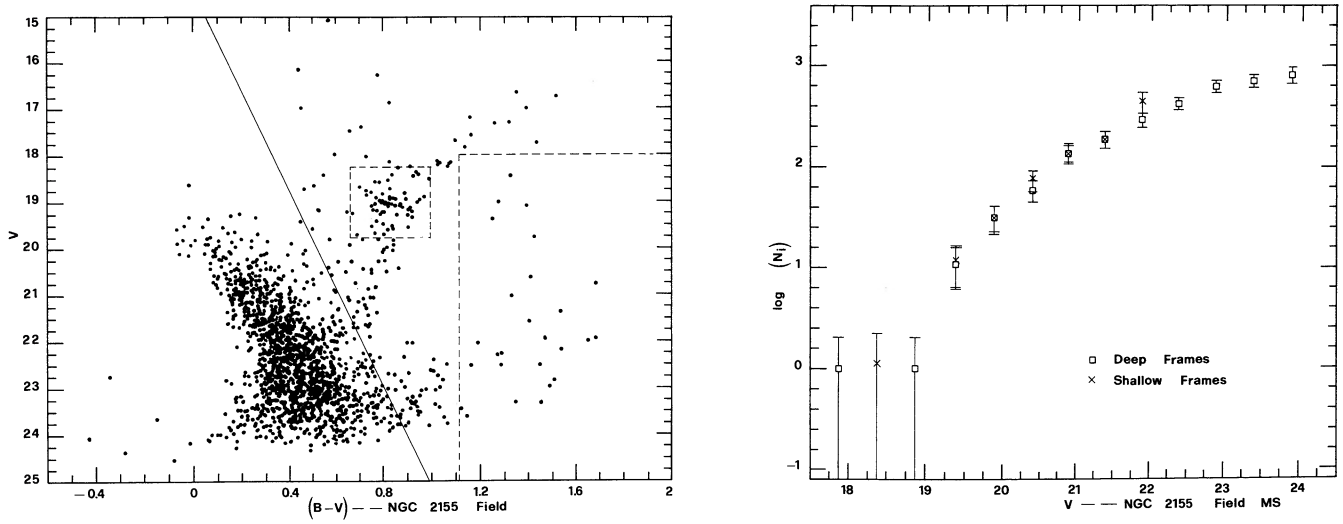

FIG. 3.—Same as in Fig. 1 but for the field near NGC 2155. The total number of stars in the red clump box is $N_{RC} = 69$.

TABLE 2

STAR COUNTS IN THE CMDs: CUMULATIVE LUMINOSITY FUNCTIONS

		NGC 1783; $N_{RC} = 118$			NGC 1866; $N_{RC} = 97$			NGC 2155; $N_{RC} = 69$		
V_{max}	V_{min}	N	N_R	N_B	N	N_R	N_B	N	N_R	N_B
15.5	15.0.....	2	1	1	0	0	0	0	0	0
16.0	15.5.....	4	3	1	6	4	2	0	0	0
16.5	16.0.....	7	6	1	13	11	2	0	0	0
17.0	16.5.....	10	9	1	14	12	2	3	3	0
17.5	17.0.....	21	19	2	22	18	4	9	9	0
18.0	17.5.....	36	31	5	36	25	11	15	14	1
18.5	18.0.....	61	48	13	59	38	21	29	28	1
19.0	18.5.....	116	86	30	132	70	62	52	50	2
19.5	19.0.....	230	150	80	245	130	115	102	94	8
20.0	19.5.....	336	177	159	341	151	190	140	109	31
20.5	20.0.....	462	188	274	511	172	339	194	120	74
21.0	20.5.....	678	204	474	727	192	535	298	130	168
21.5	21.0.....	891	219	672	1010	211	799	443	141	302
22.0	21.5.....	1180	229	951	1383	226	1157	651	147	504
22.5	22.0.....	1549	241	1308	1795	238	1557	920	158	762
23.0	22.5.....	1874	264	1610	2170	269	1901	1206	171	1035
23.5	23.0.....	1992	274	1718	2343	274	2069	1496	192	1304
24.0	23.5.....	2007	274	1733	2351	274	2077	1714	199	1515
24.5	24.0.....	...	...	...	...	...	...	1758	199	1559
25.0	24.5.....	...	...	...	...	...	...	1759	199	1560

foreground Galactic stars according to the estimated numbers of such stars from Ratnatunga & Bahcall (1985). These stars are not included in any of the LFs discussed in this paper. The total number of additional foreground stars in the range $17 < V < 23$ is 15–20, also according to the estimates of Ratnatunga & Bahcall (1985). This is a negligible contribution; thus, we have made no corrections for field stars located outside the large dashed rectangles plotted in Figures 1–3.

Throughout this paper, we assume for each field a color excess $E_{B-V} = 0.07$, $R = A_V/E_{B-V} = 3.1$, and a true distance modulus $(m - M)_0$ equal either to 18.4 or 18.6, as noted.

3. THE THEORETICAL APPROACH

For each field, synthetic CMDs were constructed using stellar evolutionary models incorporating either convective overshooting or semiconvection. An important feature of these models for the present study is the fact that they provide a homogeneous set of stellar evolutionary calculations from the ZAMS to the post-AGB stages for a large range in stellar mass. To simulate the observed field CMDs, stars were randomly placed in the synthetic CMDs according to an assumed SFR and initial mass function (IMF).

The form of the SFR used in this study is illustrated schematically in Figure 4. This is defined by the following set of parameters: τ_B, the age of the beginning of the dominant episode of star formation or "burst," τ_F, the age of the end of the burst; τ_{LMC}, the age of the LMC; S, the ratio of the post- and preburst SFR or SFR strength; and slope x of the IMF. For the sake of simplicity in the analysis below we have adopted a single value for the age of the LMC equal to 15×10^9 yr.

For the IMF we use the classical Salpeter (1955) law according to which the number of stars dN in the mass interval dM is given by

$$dN = AM^{-x}dM\,, \qquad (1)$$

where $x = 2.35$ and A is a suitable normalization constant. In our approach, x is a free parameter to be fixed by imposing certain observational constraints we describe below.

Synthetic CMDs were generated by adding stars to the color-magnitude plane until the number of stars in a well-defined region of this plane matched the observed number. Results for 30 such runs were averaged together in order to assess the magnitude of the stochastic variations that arise from observations containing a finite number of stars in any given field.

The conversion from luminosities and effective temperatures to magnitudes and colors in the UBVRI passbands are based on the relationships given by Green et al. (1987) for the metal-

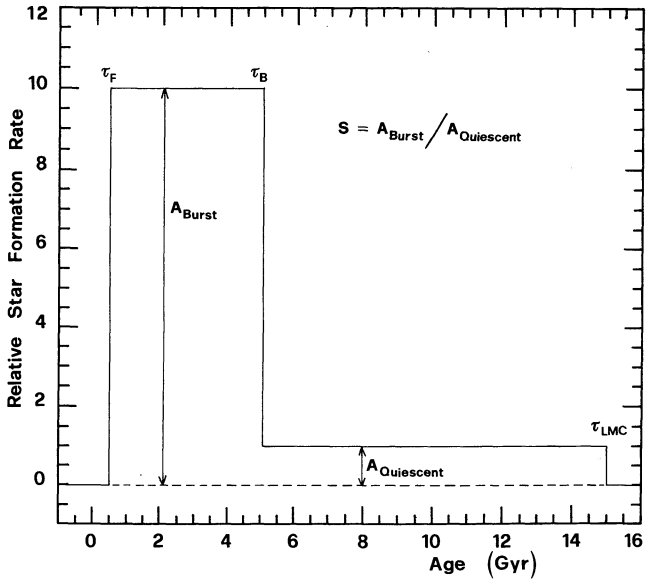

FIG. 4.—Schematic representation of the assumed form of the star formation rate in our LMC fields. The parameters are τ_B, the age of the beginning of the burst; τ_F, the age of the end of the burst; τ_{LMC}, the age of the LMC; and S, the ratio of the post- and preburst star formation rate.

TABLE 3

COMPLETENESS CORRECTIONS

A. NGC 1783 FIELD

V MAGNITUDE BIN	$(B-V)$ COLOR BIN			
	−0.3 to 0.15	0.15–0.6	0.6–1.05	1.05–1.5
≤17.12.....	1.00	1.00	1.00	1.00
17.62–17.12.....	1.00	1.00	0.97	1.00
18.12–17.62.....	1.00	1.00	0.87	1.00
18.62–18.12.....	0.99	1.00	0.81	1.00
19.12–18.62.....	0.92	0.98	0.83	0.96
19.62–19.12.....	0.83	0.89	0.85	0.85
20.12–19.62.....	0.74	0.91	0.78	0.73
20.62–20.12.....	0.71	0.83	0.61	0.62
21.12–20.62.....	0.64	0.74	0.45	0.51
21.62–21.12.....	0.62	0.58	0.35	0.39
22.12–21.62.....	0.45	0.47	0.26	0.28

B. NGC 1866 FIELD

V MAGNITUDE BIN	$(B-V)$ COLOR BIN			
	−0.3 to 0.2	0.2–0.7	0.7–1.2	1.2–1.7
≤18.12.....	1.00	1.00	1.00	1.00
18.62–18.12.....	0.97	0.98	1.00	0.97
19.12–18.62.....	0.88	0.95	1.00	0.91
19.62–19.12.....	0.79	0.91	0.94	0.80
20.12–19.62.....	0.71	0.84	0.85	0.68
20.62–20.12.....	0.65	0.76	0.72	0.55
21.12–20.62.....	0.59	0.66	0.60	0.43
21.62–21.12.....	0.56	0.56	0.47	0.32
22.12–21.62.....	0.49	0.46	0.35	0.21

C. NGC 2155 FIELD

V MAGNITUDE BIN	$(B-V)$ COLOR BIN			
	−0.2 to 0.3	0.3–0.8	0.8–1.3	1.3–1.8
≤19.12.....	1.00	1.00	1.00	1.00
19.62–19.12.....	1.00	1.00	1.00	0.98
20.12–19.62.....	0.99	0.99	0.95	0.79
20.62–20.12.....	0.93	0.93	0.86	0.66
21.12–20.62.....	0.87	0.88	0.80	0.65
21.62–21.12.....	0.81	0.82	0.72	0.64
22.12–21.62.....	0.74	0.72	0.67	0.53

licity suited to the theoretical evolutionary sequences in usage. Although other conversions can be found in the literature (see Chiosi, Bertelli, & Bressan 1988; Chiosi et al. 1989) which are perhaps more appropriate for intermediate age CMDs (like those under examination), the popular conversions by Green et al. (1987) are sufficient for our purposes.

3.1. *The Stellar Models*

Models with Semiconvection.—These models follow the classical prescription for semiconvective mixing at the border of the convective core during the central He-burning phase. The evolutionary models at the base of our study are those calculated by Fagotto (1990). They are similar to those computed by Castellani, Chieffi, & Straniero (1989) and Lattanzio (1986, 1987a, b, 1991). The set of models with semiconvection used in our analysis have the composition $Y = 0.28$ and $Z = 0.020$. This choice is forced on us because of the lack of grids of stellar models with different chemical compositions spanning the range of age and evolutionary phases required by our analysis.

Models with Core Overshoot.—Models with overshoot from the convective core are from Bertelli et al. (1985, 1986a, b, 1990) and Bressan et al. (1986). They are based on the formulation of convective overshoot developed by Bressan, Bertelli, & Chiosi (1981), in which the efficiency of overshoot is regulated by the mixing-length parameter ($\Lambda = 1$). In these models the extension of convective cores is affected by overshoot during both the core H- and He-burning phases. However, in the mass range 1–1.6 $M_\odot$, the revision of the efficiency of convective overshoot advanced by Aparicio et al. (1990) has been adopted. The point of uncertainty in modeling convective overshoot during the central H-burning phase of stars in the above mass range is related to the fact that contrary to what happens in stars of higher mass, where the convective core always recedes in mass, the convective core first increases, reaches a maximum extension, and then recedes. The question arises whether or not convective overshoot may erode the gradient in molecular weight in the region surrounding the core during the expansion phase. Aparicio et al. (1990) found that using models where this is not allowed to occur, the morphology of the CMDs of old open clusters such as M67 and King 2 can be reproduced more precisely. Therefore, we adopt these types of evolutionary models. Without going into a detailed discussion of the properties of overshoot models, it is appropriate to recall a few basic points. The core H-burning phase runs at higher luminosities, extends to lower effective temperatures, and lasts longer than in classical models. These effects become less pronounced in the mass range 1–1.6 $M_\odot$, although the core He-burning phase remains overluminous and is short-lived compared to classical models. This implies that the ratio of the numbers of stars burning He in their cores divided by stars still burning H in their cores is significantly smaller than in the classical (semiconvective) models. The models with core overshoot adopted here have the chemical composition $Y = 0.25$ and $Z = 0.004$, which is likely suited to the LMC field stars (see the study of Olszewski et al. (1991) on the metallicity of clusters in the LMC).

Remarks on the Chemical Parameters.—Because of the limitations on the available data bases of stellar tracks covering the whole range of masses and evolutionary phases required by our analysis, we were forced to use semiconvective models with a composition different from that of overshoot models and also not fully appropriate for field stars of the LMC. The obvious question may be posed at what extent the final results will be affected by this limitation in the choice of the chemical composition. The method at the base of our analysis essentially rests on star counts in different areas of the CMD (see below). The many existing stellar models calculated with approximately the same input physics but different chemical abundances ensure us that within a given evolutionary scheme the lifetimes of the various phases are only marginally affected by variation in the chemical parameters, the metallicity in particular. To this purpose compare models of the same mass but different chemical composition, for example, Lattanzio (1991) for semiconvection and Bertelli et al. (1986a) for overshoot. The lifetimes are by far more affected by the choice of the evolutionary scheme (either semiconvection or overshoot) than by the precise values of the chemical abundances in use. Therefore, although other chemical compositions are probably more appropriate for the LMC field stars, the main results of our study are not to be too severely affected by the above limitations in the choice of the chemical parameters.

3.2. *The Number Ratios R_1, R_2, and R_3: Definitions*

The models and observations were compared in three ways: (1) through the detailed morphology of the CMDs; (2) through

the MS and post-MS differential and integrated luminosity functions, corrected for incompleteness; and (3) through three ratios of star counts in different areas of the CMD. The latter comparison is especially useful because it is relatively insensitive to uncertainties in the choice of chemical parameters, which would affect the colors of the stars rather than their relative lifetimes.

The Ratio R_1.—For $M_V = 3$, main-sequence stars are clearly separated from the evolved stars (subgiants and giants) in all of the field CMDs. Thus we define R_1 as the number ratio of main-sequence stars to red giants, both brighter than $M_V = 3$. The separation of evolved from main-sequence stars is based on the eye-drawn line plotted in the three CMDs (Figs. 1, 2, and 3). R_1 is expected to depend weakly on τ_B, much more strongly on τ_F, and much less on the IMF slope x. It is also expected to depend on the strength S of the burst in the SFR.

The Ratio R_2.—The parameter R_2 is defined as the ratio between the number of red giants brighter than $M_V = 1.5$ (i.e., just below the red giant clump) and the number of red giants in the magnitude interval $1.5 \leq M_V \leq 3$. This parameter is designed to distinguish core He-burning stars from stars ascending the red giant branch. The ratio R_2 turns out to depend mainly on the parameters τ_B, S, and x, and weakly on τ_F.

The Ratio R_3.—Similarly, the parameter R_3, is meant to estimate the proportions of old and young main-sequence stars. Specifically, for a fixed magnitude limit M_{VB}, R_3 is defined as the ratio of stars located in the magnitude range $3 \geq M_V \geq M_{VB}$ and those brighter than M_{VB}. Although M_{VB} should only be defined after inspecting the morphology of the stars in the CMD, for the sake of simplicity we have assumed $M_{VB} = 1.5$, the same as for the red stars; this choice is adequate for our analysis. It is easy to understand that R_3 is expected to depend weakly on τ_B and S, and strongly on τ_F and IMF slope x.

The values of the three parameters that result from our star counts corrected for completeness are given in Table 4 together with their uncertainties for two assumptions of the true distance modulus, i.e., $(m-M)_0 = 18.4$ and $(m-M)_0 = 18.6$. The uncertainties mostly reflect the counting fluctuations. We estimate that random and systematic photometric errors and nonuniformity of the background have a small effect on the star counts.

3.3. *The Number Ratios R_1, R_2, and R_3: Analysis*

Large grids of synthetic CMDs and LFs have been computed to single out the dependence of the number ratios R_1, R_2, and R_3 on the four basic parameters τ_B, τ_F, S, and x. An estimate of τ_F, is given by the termination magnitudes of the main-sequence bands in the three CMDs, indicating that τ_F may vary from field to field in the age range of several 10^8 yr. The exact value depends on the assumed chemical composition and underlying stellar models. At a given termination magnitude, τ_F is expected to decrease going from models with core overshoot to the classical ones with semiconvection. No direct information is available for the other three parameters. In the following, we will discuss a few illustrative examples first for models with core overshoot, and then for models with semiconvection. In all of the examples discussed below, we give the values of R_1, R_2, and R_3 derived from averaging the results of 30 simulations together with the variance for each ratio. This allows us to estimate the uncertainties introduced by stochastic effects in our limited samples of field stars.

TABLE 4

STAR COUNTS: THE OBSERVATIONAL RATIOS R_1, R_2, AND R_3

Field	R_1	R_2	R_3
Distance Modulus $(m-M)_0 = 18.4$			
NGC 1783.....	3.71 ± 0.25	3.33 ± 0.68	3.67 ± 0.39
NGC 1866.....	5.01 ± 0.34	1.90 ± 0.34	4.04 ± 0.44
NGC 2155.....	2.64 ± 0.24	2.81 ± 0.70	8.44 ± 1.80
Distance Modulus $(m-M)_0 = 18.6$			
NGC 1783.....	4.21 ± 0.29	2.96 ± 0.54	3.58 ± 0.33
NGC 1866.....	6.04 ± 0.41	1.79 ± 0.34	3.54 ± 0.31
NGC 2155.....	3.38 ± 0.31	2.91 ± 0.70	6.68 ± 1.16

Overshoot Models.—Figures 5, 6, and 7 show the dependence of the ratios R_1, R_2, and R_3, respectively, at a given τ_F and SFR strength S, and for two values of x. In these examples, $\tau_F = 5 \times 10^8$ yr, as indicated by the termination magnitude of the main-sequence band of the NGC 1783 and NGC 1866 fields, and $S = 10$. An older age is more appropriate for the NGC 2155 field described in more detail later on. The left panel of each figure is for $x = 2.35$, whereas the right panel is for $x = 1.35$. Figures 8, 9, and 10 show the same quantities but for a burst strength $S = 5$. Comparing Figures 5 and 8, it is evident that, if τ_F is known, R_1 is a good indicator of τ_B and S, but insensitive to x. The largest dependence on S is for τ_B in the range 1×10^9 yr to $(4–5) \times 10^9$ yr. The ratio R_2 (see Figs. 6 and 9) for all combinations of S and x peaks at τ_B approximately equal to $(2–3) \times 10^9$ yr, which corresponds to the age (initial star mass) where the transition from quiet core He-ignition to core He-flash occurs. In this age range (say at about 2.5×10^9 yr), R_2 shows also the maximum sensitivity to x. Therefore R_2 is a good indicator of τ_B, S, and x, but very poorly constrains τ_F. The ratio R_3 tends to an asymptotic value with increasing τ_B that depends on x. The dependence of R_3 on the burst strength S is almost negligible (see Figs. 7 and 10). Figure 11 shows the variation of R_3 as function of τ_F, τ_B, and x, at given S. The values of τ_B are indicated along each curve. It is noteworthy that for τ_B older than about 3×10^9 yr, R_3 is almost insensitive to this parameter. Because τ_F can be derived from the main-sequence termination magnitude, it follows that R_3 is a sensitive indicator of the IMF slope x.

Semiconvective Models.—Although the semiconvective models at our disposal have a chemical composition that is not strictly appropriate for the LMC field stars, they are still useful to understanding how the three diagnostic ratios depend on the physics of the underlying evolutionary models. Owing to the different relations between mass, luminosity, and age used by semiconvective and overshoot models, different choices for τ_F must be made. For the semiconvective models, the termination magnitudes of the main sequence of the NGC 1783 and NGC 1866 fields indicate ages of the order of $(1–2) \times 10^8$ yr. The examples we will present are for $\tau_F = 1 \times 10^8$ yr and $S = 10$. The dependence of R_1, R_2, and R_3 on τ_B and x are shown in Figures 12, 13, and 14, respectively. As expected, the general behavior is the same as for the previous cases, even if there are many quantitative differences. Comparing Figure 5 and 12, we notice that R_1 now peaks at much younger ages (5×10^8 yr), and the peak itself is less pronounced by about a factor of 2 compared to overshoot models. This can be ascribed to the different core He- to H-burning lifetime ratio, which is much higher for semiconvective models. The same

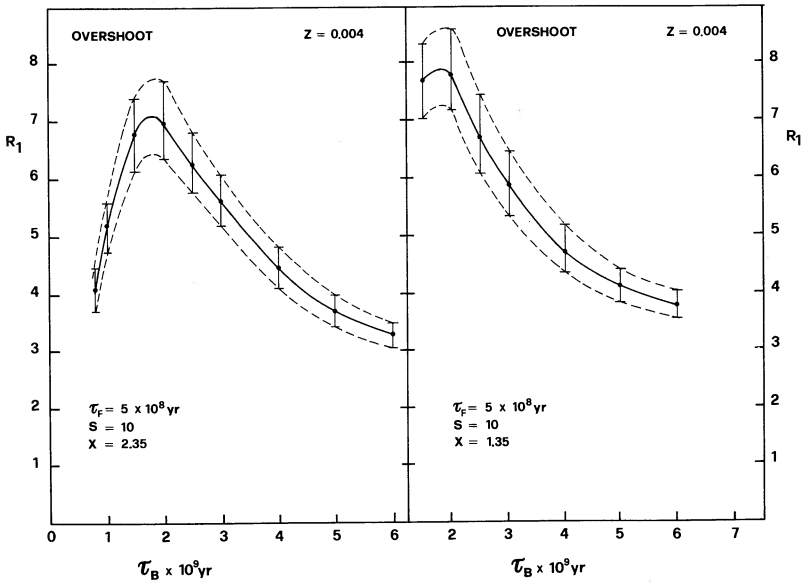

FIG. 5.—The R_1 vs. τ_B relationship for models with convective overshoot and chemical composition $Y = 0.25$ and $Z = 0.004$. The relative amplitude of the burst in the SFR is $S = 10$, and the final age of the burst is $\tau_F = 5 \times 10^8$ yr. *Left panel*: IMF slope $x = 2.35$; *right panel*: $x = 1.35$. The central (*solid*) line of each relation is the mean value of 30 simulations. Vertical bars show the variance. Dashed lines define the band in the R_1 vs. τ_B relation generated by stochastic effects in the number of stars.

considerations already made for R_2 derived from overshoot models hold for R_2 obtained from models with semiconvection (compare Figs. 6 and 13). The peak value of R_2 is now shifted to 10^9 yr which is approximately the lifetime of the transition mass (2.2 $M_\odot$) between quiet core He-burning and core He-flash. The ratio R_3 shows the same trend as noted for the overshoot models (compare Figs. 14 and 7).

The Role of τ_F.—As already stated, the main-sequence band of the NGC 2155 field terminates at a magnitude fainter than in the other fields. This indicates an older age for τ_F, say, (1.2–1.3) $\times$ 10^9 yr for models with overshoot or 5×10^8 yr for models with semiconvection. The effect of an older age on the ratios R_1, R_2, and R_3 is shown in Figure 15 (overshoot) and Figure 16 (semiconvection) for $S = 10$ and $x = 2.35$. As expected, although the behavior is similar to that of the previous cases, the peak value of R_1 is significantly smaller (see Fig. 5). Therefore, R_1 depends sensitively on τ_F, as well as on τ_B and S. This can be explained by noting that a burst is a summation of many isochrones of different age weighted by the IMF. From the isochrone tabulation of Bertelli et al. (1990) we see that R_1 increases from 6.7 for the age of 2×10^9 yr to 29.1 for the age of 7×10^8 yr. Similar reasoning explains why R_2 remains approximately constant as τ_F increases. This is mainly caused by the rapid decrease of the core He-burning lifetime

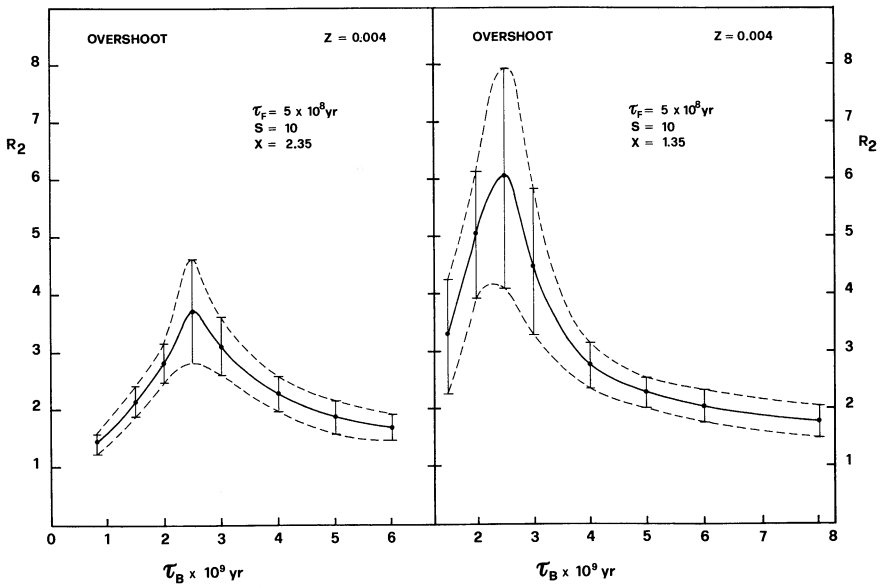

FIG. 6.—The R_2 vs. τ_B relationship for models with convective overshoot and chemical composition $Y = 0.25$ and $Z = 0.004$. See Fig. 5 for other values and symbols.

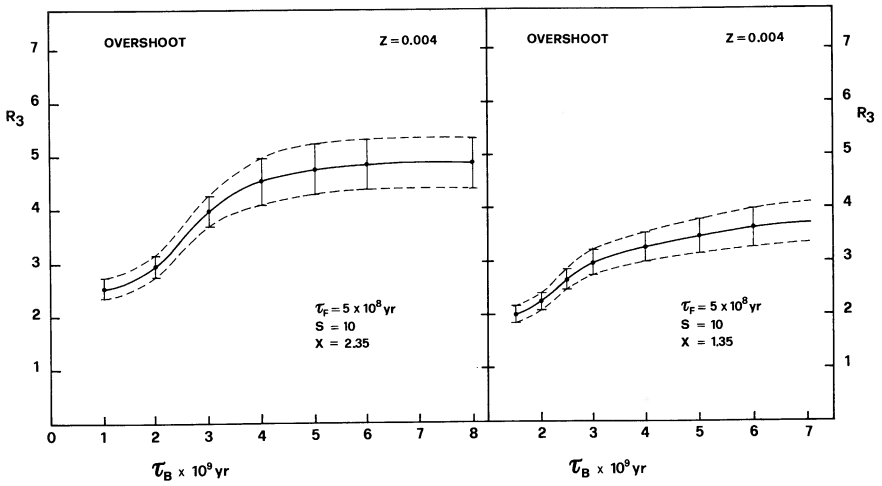

FIG. 7.—The R_3 vs. τ_B relationship for models with convective overshoot and chemical composition $Y = 0.25$ and $Z = 0.004$. See Fig. 5 for other values and symbols.

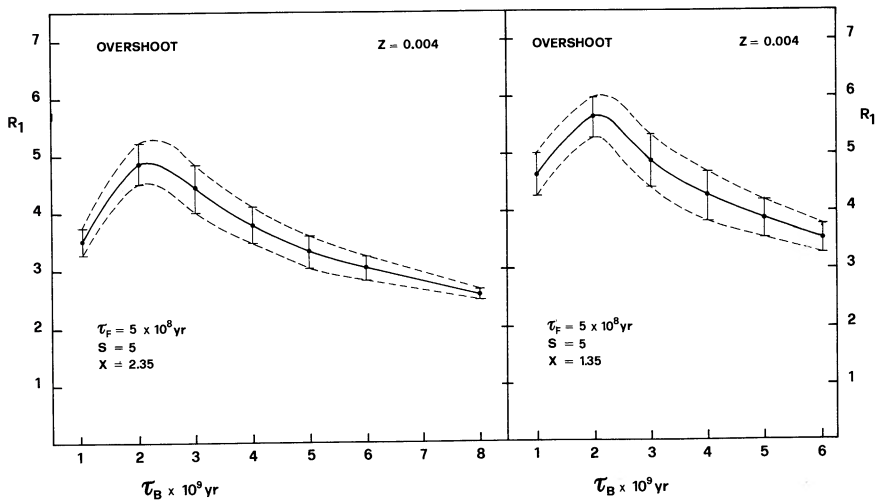

FIG. 8.—Same as in Fig. 5 but for the relative amplitude of the burst $S = 5$

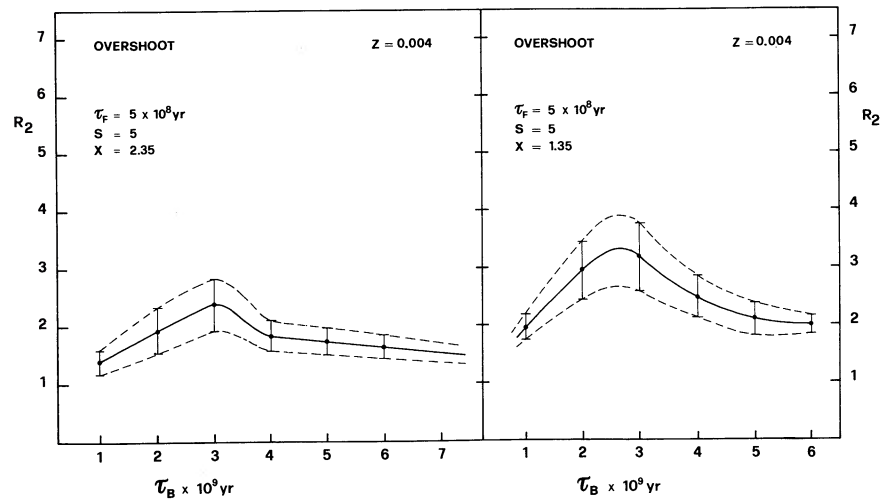

FIG. 9.—Same as in Fig. 6 but for the relative amplitude of the burst $S = 5$

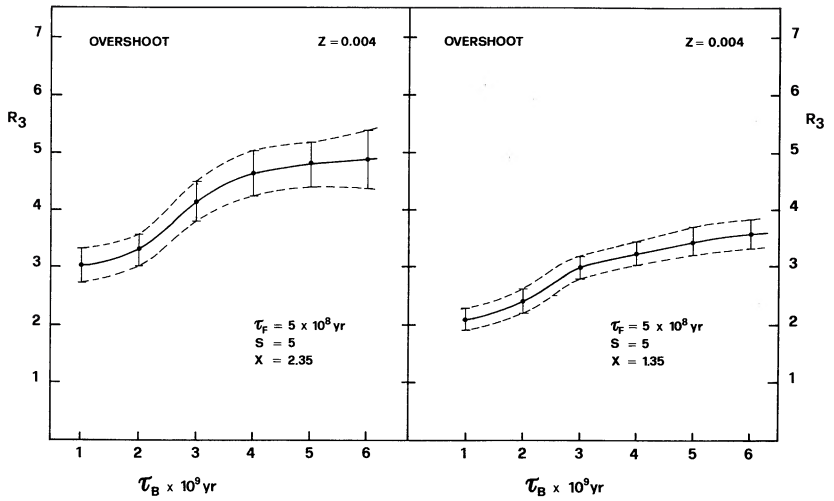

FIG. 10.—Same as in Fig. 7 but for the relative amplitude of the burst $S = 5$

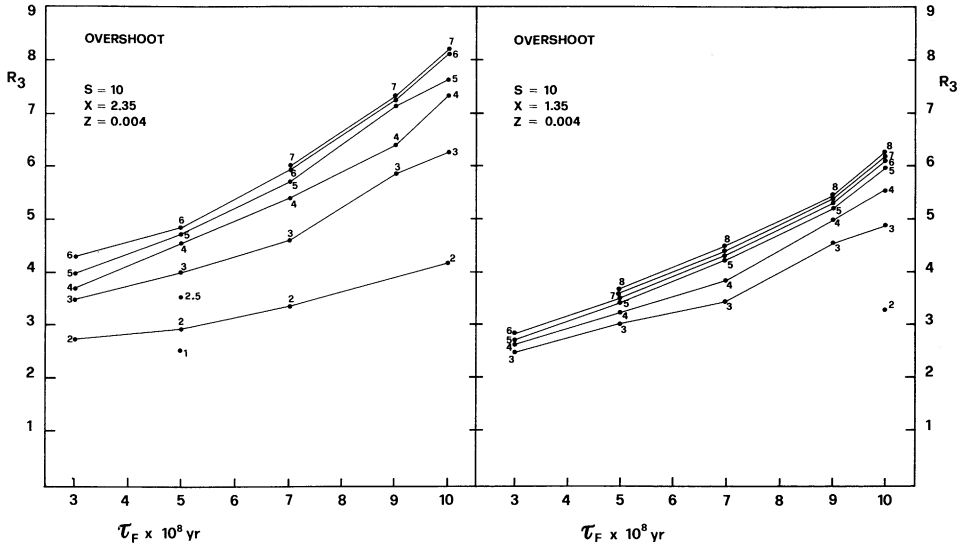

FIG. 11.—The R_3 vs. τ_F relationship for models with convective overshoot and chemical composition $Y = 0.25$ and $Z = 0.004$. The relative amplitude of the burst in the SFR is $S = 10$. *Left panel*: IMF slope $x = 2.35$; *right panel*: $x = 1.35$. Each line corresponds to a different choice for τ_B as indicated. Values of τ_B are expressed in units of 10^9 yr. Each line is the mean of 30 simulations, and no stochastic effects are shown.

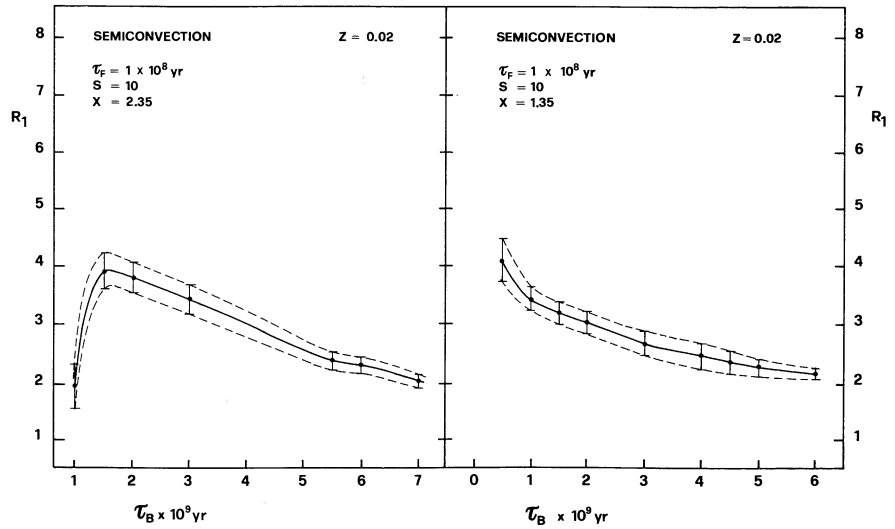

FIG. 12.—The R_1 vs. τ_B relationship for models with semiconvection and chemical composition $Y = 0.28$ and $Z = 0.020$. See Fig. 5 for other values and symbols.

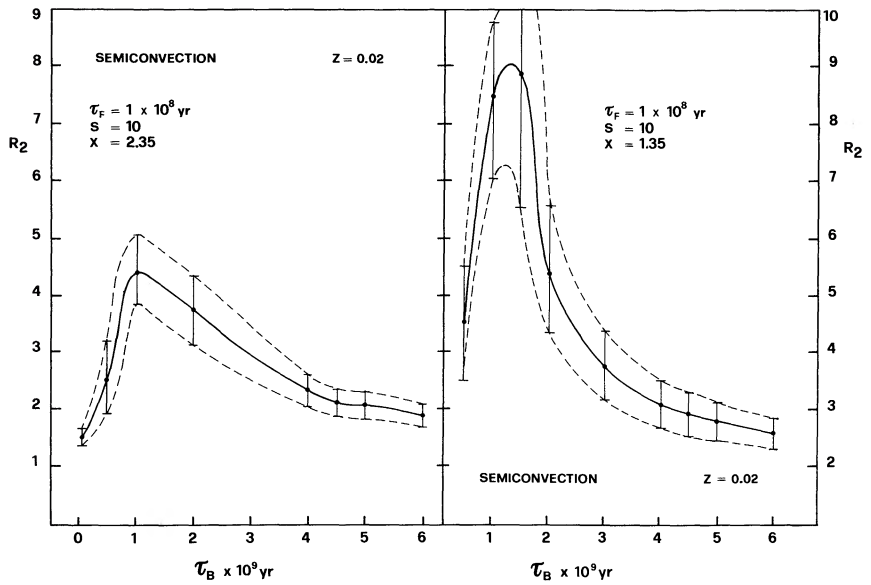

FIG. 13.—The R_2 vs. τ_B relationship for models with semiconvection and chemical composition $Y = 0.28$ and $Z = 0.020$. See Fig. 5 for other values and symbols.

with the mass of the star, and the decrease in the number of massive stars caused by the slope of the IMF. Finally, it is apparent that an increase in τ_F leads to a drastic increase in R_3, together with a change in the functional dependence of this ratio with τ_B.

Presence of Binary Stars.— We have considered the possibility that a fraction of the stars in each sample are unresolved binaries. Synthetic CMDs have been generated assuming that binary stars amount to 25% of the total and that their mass ratios lie in the range 0.8–1.2. The inclusion of binary stars broadens the main-sequence band, brightens the termination magnitude by about 0.7 mag, and scatter stars into the so-called Hertzsprung gap between the main sequence and the red giant branch. For more details on this topic see Maeder (1974) and Vallenari et al. (1991a, b). In the analysis below we will present cases in which binary stars are included.

Other Laws of Star Formation.—Many CMDs and LFs have been generated assuming different sorts of SFR. These simulations are not shown here for the sake of brevity. Nevertheless, the dependence of the distribution of stars in the CMD on the underlying SFR can be easily understood, at least from a qualitative point of view. Neglecting variations in the chemical composition, the CMDs of Figures 1–3 can be interpreted as the convolution of many generations of stars, each of which has a different age and relative weight determined by the past history of the SFR. Assuming a narrow age spread within each generation, the corresponding distribution of stars in the CMD can be approximated by an isochrone of given age. Therefore the problem reduces to convolve isochrones of different age into a SFR. With the aid of the isochrone and luminosity function (number of stars) tabulations of Bertelli et al. (1990), we expect that both a SFR constant over the galaxian age and a SFR declining exponentially from the past to the present would predict far too many subgiant stars (SGB) than are observed. Specifically, with this kind of SFR, the number of old, low-mass stars dominate the population, and thus, owing

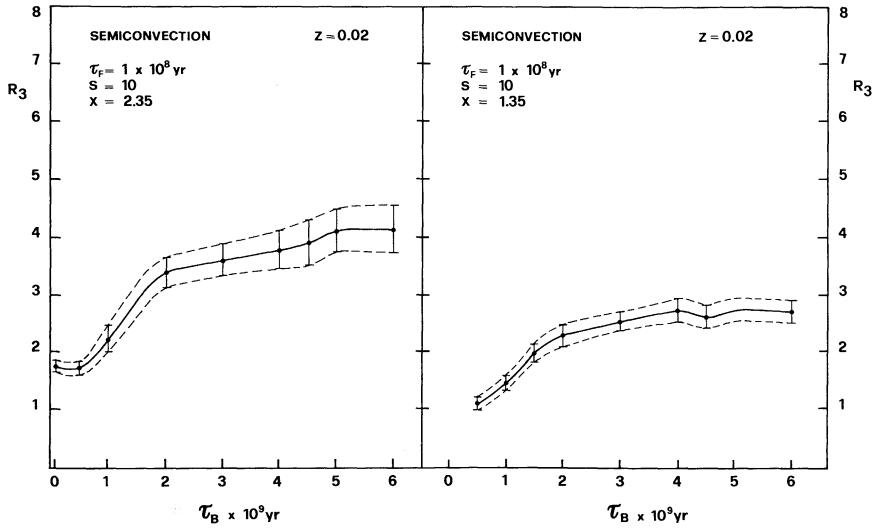

FIG. 14.—The R_3 vs. τ_B relationship for models with semiconvection and chemical composition $Y = 0.28$ and $Z = 0.020$. See Fig. 5 for other values and symbols.

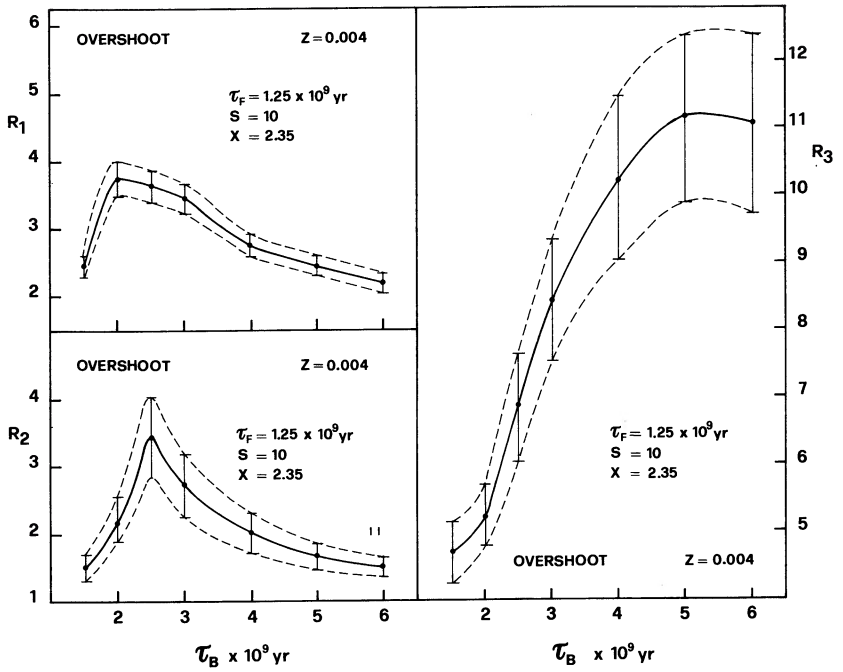

FIG. 15.—The R_1 (*left top panel*), R_2 (*left bottom panel*), and R_2 (*right panel*) vs. τ_B relationships for models with convective overshoot and chemical composition $Y = 0.25$ and $Z = 0.004$. These relations differ from the corresponding ones of Figs. 5, 6, and 7 for the value of $\tau_F = 1.25 \times 10^9$ yr. They are thought to be appropriate for the somewhat older stellar content of NGC 2155. See Fig. 5 for other values and symbols.

to the relatively long lifetime of stages beyond the core H-burning phase and prior to the RGB tip, the number of SGBs is expected to be a considerable fraction of the total. This would immediately reflect on a ratio R_2 much lower than observed. This conclusion holds virtually regardless of what other model parameters are employed. Similarly, a SFR that monotonically increases to the present epoch would yield results that are very close to those obtained with the burst hypothesis.

4. COMPARISONS OF MODELS WITH THE OBSERVATIONS

4.1. *The Method*

We begin by deriving an estimate of τ_F based on the location of the main-sequence termination magnitude assuming a

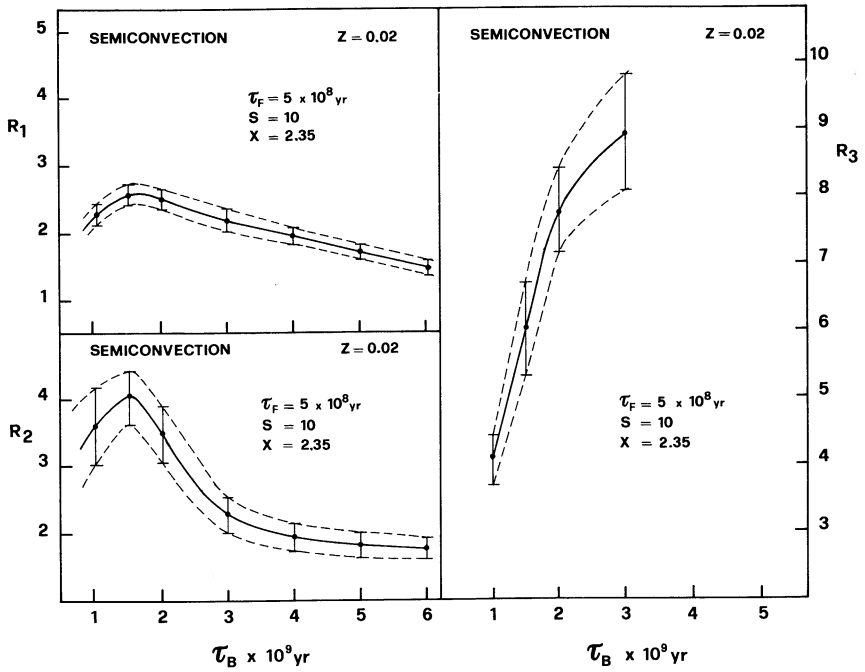

FIG. 16.—The R_1 (*left top panel*), R_2 (*left bottom panel*), and R_3 (*right panel*) vs. τ_B relationships for models with semiconvection and chemical composition $Y = 0.28$ and $Z = 0.020$. These relations differ from the corresponding ones of Figs. 8, 9, and 10 for the value of $\tau_F = 5 \times 10^8$ yr. They are thought to be appropriate for the somewhat older stellar content of NGC 2155. See Fig. 5 for other values and symbols.

chemical composition consistent with the mean color of the main sequence. We then fix the burst strength S and IMF slope x, and search for a value of τ_B that yields values of R_1, R_2, and R_3 that match the observed ratios. Since S and x are arbitrarily chosen, the three values of τ_B so derived do not agree in general. The procedure is iterated by varying S and x until coincidence between the three τ_B values is found. This leads to the determination of the basic parameters of the SFR, namely the relative intensity of the burst (S) and the epoch when the burst began, τ_B.

Because the CMDs contain a relatively small number of stars, stochastic effects are likely to be significant. Thus, in comparing the theoretical and observed diagnostic ratios R_1, R_2, and R_3, we have explicitly taken into account these stochastic uncertainties, the size of which is given by $2\Delta R_i$ obtained from the data in Table 4. The corresponding uncertainty in the derived value of τ_B follows directly. To illustrate the point, we examine in some detail the case of NGC 1866. Figure 17 schematically shows the possible intersections of the theoretical bands obtained from models with overshoot with the corresponding observational ones, for a fixed value of S and different values of x. In this example we make use of the observational ratios R_1, R_2, and R_3 obtained assuming the distance modulus of $(m-M)_0 = 18.4$. Figure 18 shows the same but for a different choice of S. Acceptable values of τ_B are indicated in Figures 17 and 18 by vertical bars drawn with different symbols. The long thick bars show the domain of τ_B given by the intersection of the theoretical and observational bands (variance and errors included). The dashed bars correspond to the intersection of the observational R_i *without* errors with the theoretical bands *with* variance. Finally, the short thin bars show the intersection of the observational ratios *without* errors with the theoretical lines *without* variance. The shaded areas show the intervals of τ_B where solutions common to the three R_i values can be found.

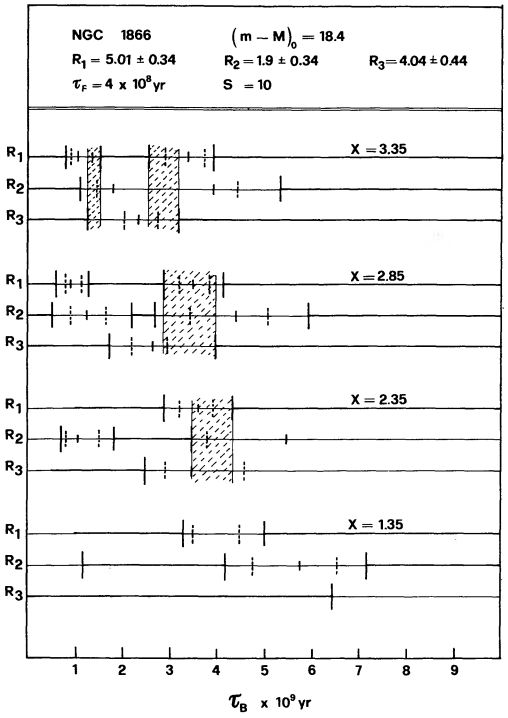

FIG. 17.—Solutions for the NGC 1866 field using models with convective overshoot ($Y = 0.25$ and $Z = 0.004$) and assuming the distance modulus $(m-M)_0 = 18.4$. The observational values of R_1, R_2, and R_3 are indicated in the top panel. These solutions are for $\tau_F = 4 \times 10^8$ yr, appropriate for the NGC 1866 field, and relative amplitude of the burst $S = 10$. Each panel differs from the others for the slope of the IMF as indicated. The domains of existence of the solutions are indicated by vertical bars drawn with different symbols. The thick long bars show the domain of τ_B given by the intersection of the theoretical and observational bands. Dotted bars correspond to the intersection of the observational R_i without errors with the theoretical bands. Thin short bars show the intersection of the observational ratios without errors with the theoretical lines without variance. Shaded areas show the intervals of τ_B where common solutions are found.

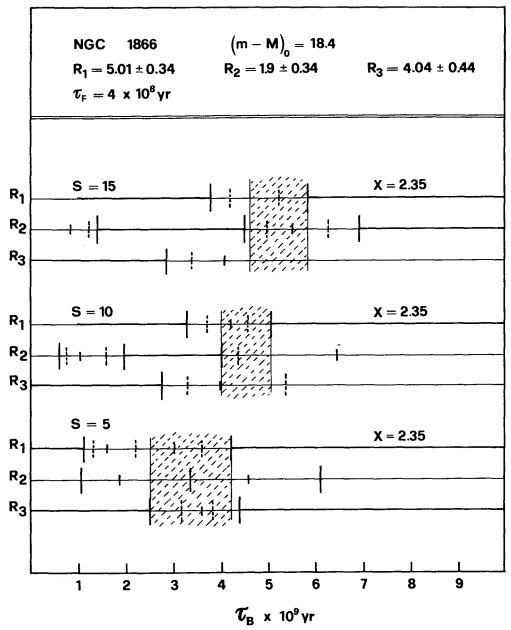

FIG. 18.—Same as in Fig. 17 but different values of the parameter S in the SFR.

In order to understand the results presented in Figures 17 and 18, consider the part of Figure 17 for $x = 2.85$, $S = 10$, and $\tau_F = 4 \times 10^8$ yr. The shaded area indicates that τ_B lies in the range $(2.9\text{–}4.0) \times 10^9$ yr because only then do the theoretical estimates of R_1, R_2, and R_3 match the observed values. In addition to this, the other cases shown in Figure 17 illustrate that τ_B changes systematically with the IMF slope, x. There are multiple solutions for τ_B for $x = 3.35$. For $x = 2.85$ and 2.35, τ_B becomes systematically larger. For $x = 1.35$, there is no solution at all.

4.2. *Hunting for Solutions*

Using the procedure described above, we have determined all possible solutions for the fields. The results are given in Tables 5A through 6B. Table 5A is for overshoot models and a distance modulus $(m-M)_0 = 18.4$, while Table 5B is for the same models but for a distance modulus $(m-M)_0 = 18.6$. Similarly, Tables 6A and 6B refer to semiconvective models and a distance modulus $(m-M)_0 = 18.4$ and 18.6, respectively. Recall that a different choice for the distance modulus alters the observational ratios R_1, R_2, and R_3 (see Table 4) because they are defined by absolute magnitude limits. In Tables 5A–6B we show also solutions obtained with the inclusion of binary stars (cases labeled BS). As expected, the effect of binary stars is negligible. This is simply due to the fact that our ratios R_1, R_2, and R_3 are constructed by counting stars over broad

TABLE 5A

ALLOWED VALUES FOR τ_B: MODELS WITH CONVECTIVE OVERSHOOT

		τ_B			
τ_F	S	$x = 3.35$	$x = 2.85$	$x = 2.35$	$x = 1.35$
Field NGC 1783 $Y = 0.25$ $Z = 0.004$ $(m-M)_0 = 18.4$					
0.4.....	5	...	...	...	...
	10	...	...	...	...
	10 BS	...	...	4.25–4.50	...
	15	...	...	...	...
0.5.....	5	...	...	...	3.70–4.50
	10	...	...	...	...
	10 BS	...	...	3.90–4.85	4.50–5.75
	15	...	...	...	...
Field NGC 1866 $Y = 0.25$ $Z = 0.004$ $(m-M)_0 = 18.4$					
0.4.....	5	...	...	2.25–3.65	...
	10	1.25–1.50	2.85–4.00	3.50–4.35	...
	10	2.55–3.15	...	...	...
	10 BS	2.30–3.70	...	3.90–4.00	...
	15	...	...	4.00–5.00	...
0.5.....	5	...	...	2.00–3.30	...
	10	1.05–1.90	...	3.50–4.10	...
	10	2.10–2.65	...	...	...
	10 BS	...	3.50–4.25	3.80–4.00	...
	15	...	...	...	...

		τ_B		
τ_F	S	$x = 2.35$	$x = 1.85$	$x = 1.35$
Field NGC 2155 $Y = 0.25$ $Z = 0.004$ $(m-M)_0 = 18.4$				
1.0.....	10	4.35–5.00	...	...
1.25.....	10	3.50–4.35	3.60–5.10	...
1.50.....	10	2.00–2.90	...	2.25–3.85

NOTES.—Empty values in the rows stand for the lack of solutions. BS means that binary stars are taken into account. Ages are in units of 10^9 yr.

ranges of magnitudes and colors, thus encompassing all effects caused by the probable existence of a certain percentage of binary stars. An inspection of Tables 5A through 6B reveals that models with overshoot and low metal content yield the largest number of solutions, whereas semiconvective models offer many fewer possibilities. Although this might be partly ascribed to the inadequate chemical composition, we are more inclined to attribute this to inadequacies in the models themselves because the ratio of the core He-burning to core H-burning lifetimes is in conflict with the star counts. The entries in Table 5A (based on overshoot models and short distance modulus) show that various solutions are allowed for NGC 1866 and NGC 2155. Finding a valid solution for the NGC 1783 field is more difficult unless a significant contribution by binary stars is included. The difficulty with this field derives from the conflicting values of R_1 and R_2. Specifically, while the large value of R_2 indicates a recent age for τ_B, the low value of R_1 suggests an old age for τ_B.

Based on the above discussion and the data in Table 5A, we conclude that the star counts for each field are consistent with $x = 2.35$ and $S = 10$. For the value of τ_F appropriate for each field, a single burst age, $\tau_B \sim 4 \times 10^9$ yr, is consistent with all the data. More precisely, we get the following results: for NGC 1783 $\tau_F = 5 \times 10^8$ yr and $3.9 \times 10^9 \leq \tau_B \leq 4.8 \times 10^9$ yr, for NGC 1866 $\tau_F = 5 \times 10^8$ yr and $3.5 \times 10^9 \leq \tau_B \leq 4.1 \times 10^9$ yr, and finally for NGC 2155 $\tau_F = 1.25 \times 10^8$ yr and $3.5 \times 10^9 \leq \tau_B \leq 4.3 \times 10^9$ yr. With the distance modulus $(m-M)_0 = 18.4$, the overshoot models, and the low metallicity, the dominant star formation activity began in the three fields at about 4×10^9 yr ago but ended at slightly different times. If we consider the distance modulus $(m-M)_0 = 18.6$, the solutions (when they exist) yield different ranges for acceptable values for τ_B, IMF slopes, and burst strengths compared to the case based on a distance modulus $(m-M)_0 = 18.4$. More importantly, under any reasonable assumptions for the model parameters, we find no common value of τ_B for all three fields for a given set of values of S and x (Table 5B).

Repeating the same analysis for the case of stellar models with semiconvection (Tables 6A and 6B for the short and long distance modulus, respectively) we find the following results. If the distance modulus $(m-M)_0 = 18.4$ is adopted, a solution common to NGC 1783 and NGC 2155 exists for $S = 10$, $x = 2.35$, $\tau_B = 2 \times 10^9$ yr and $\tau_F = 1 \times 10^8$ yr in the case of NGC 1783, and $\tau_F = 5 \times 10^8$ yr for NGC 2155 (see the data of Table 6A). Because semiconvection models are being used, it is not surprising that the ages are systematically younger than the corresponding cases with overshoot models. However, for semiconvection models, we cannot find any solution for τ_B in the case of the NGC 1866 field due to the large observed value of R_1. For a distance modulus of $(m-M)_0 = 18.6$, we cannot find any solutions for τ_B for the NGC 1866 or NGC 2155

TABLE 5B

ALLOWED VALUES FOR τ_B: MODELS WITH CONVECTIVE OVERSHOOT

		τ_B			
τ_F	S	$x = 3.35$	$x = 2.85$	$x = 2.35$	$x = 1.35$
Field NGC 1783 $Y = 0.25$ $Z = 0.004$ $(m-M)_0 = 18.6$					
0.4.....	5	...	...	2.60–3.35	...
	10	...	...	3.90–4.35	4.40–5.50
	10 BS	...	...	3.70–5.50	...
	15	...	...	...	...
0.5.....	5	...	...	2.30–3.25	3.25–5.00
	10	...	...	...	3.75–5.40
	10 BS	...	3.25–3.40	3.35–4.65	4.50–6.00
	15	...	...	...	...
Field NGC 1866 $Y = 0.25$ $Z = 0.004$ $(m-M)_0 = 18.6$					
0.4.....	5	...	...	1.60–2.45	...
	10	1.10–2.60	1.40–1.90	...	...
	10 BS	1.40–2.75	...	...	...
	15	...	...	...	...
0.5.....	5	...	...	...	...
	10	1.30–2.15	...	...	...
	10 BS	...	...	...	...
	15	...	...	...	...

		τ_B		
τ_F	S	$x = 2.35$	$x = 1.85$	$x = 1.35$
Field NGC 2155 $Y = 0.25$ $Z = 0.004$ $(m-M)_0 = 18.6$				
1.00.....	10	3.00–4.55	...	3.35–5.20
1.25.....	10	2.00–3.20	2.25–3.80	...
1.50.....	10	2.00–2.40	...	1.90–2.70

NOTES.—Empty values in the rows stand for the lack of solutions. BS means that binary stars are taken into account. Ages are in units of 10^9 yr.

TABLE 6A

ALLOWED VALUES FOR τ_B: MODELS WITH SEMICONVECTION

		τ_B			
τ_F	S	$x = 3.35$	$x = 2.85$	$x = 2.35$	$x = 1.35$
Field NGC 1783 $Y = 0.28$ $Z = 0.020$ $(m-M)_0 = 18.4$					
0.1.....	5	...	...	...	...
	10	1.00–1.75	...	1.60–2.55	...
	15	...	...	1.80–2.60	...
0.3.....	5	...	...	...	...
	10	...	...	...	...
	15	...	...	...	...
Field NGC 1866 $Y = 0.28$ $Z = 0.020$ $(m-M)_0 = 18.4$					
0.1.....	5	...	...	...	...
	10	...	...	...	...
	15	...	...	...	...
0.3.....	5	...	...	...	...
	10	...	...	...	...
	15	...	...	...	...
Field NGC 2155 $Y = 0.28$ $Z = 0.020$ $(m-M)_0 = 18.4$					
0.5.....	10	...	...	1.70–2.85	...

NOTES.—Empty values in the rows stand for the lack of solutions. BS means that binary stars are taken into account. Ages are in units of 10^9 yr.

TABLE 6B

ALLOWED VALUES FOR τ_B: MODELS WITH SEMICONVECTION

		τ_B			
τ_F	S	$x = 3.35$	$x = 2.85$	$x = 2.35$	$x = 1.35$
Field NGC 1783 $Y = 0.28$ $Z = 0.020$ $(m-M)_0 = 18.6$					
0.1.....	5	...	...	...	...
	10	1.00–1.65	...	...	...
	15	...	...	...	...
0.3.....	5	...	...	...	...
	10	...	...	...	...
	15	...	...	...	...
Field NGC 1866 $Y = 0.28$ $Z = 0.020$ $(m-M)_0 = 18.6$					
0.1.....	5	...	...	...	...
	10	...	...	...	...
	15	...	...	...	...
0.3.....	5	...	...	...	...
	10	...	...	...	...
	15	...	...	...	...
Field NGC 2155 $Y = 0.28$ $Z = 0.020$ $(m-M)_0 = 18.6$					
0.5.....	10	...	...	...	...

NOTES.—Empty values in the rows stand for the lack of solutions. BS means that binary stars are taken into account. Ages are in units of 10^9 yr.

fields; for the NGC 1783 field we derive $\tau_F = 1 \times 10^8$ yr and τ_B in the range 1.0×10^9 yr to 1.6×10^9 yr, for $S = 10$ and $x = 3.35$.

5. DISCUSSION AND CONCLUSIONS

Numerous SFR-sensitive indices can be measured from the field star CMDs and LFs. Particularly useful are the starcount ratios R_1, R_2, and R_3 which are found to be able to constrain the SFR of LMC field stars. The method we propose is of general use and could be applied to other fields of the LMC to trace back the history of star formation in this galaxy.

The primary difference among the observed fields is that the youngest stars in the NGC 2155 field (τ_F) are significantly older than the youngest stars in the NGC 1783 field, while the youngest stars in the NGC 1866 are younger than the corresponding stars in the NGC 1783 field. This is not merely a stochastic effect resulting from the different total number of stars in the three fields, but reflects a true difference in the number of bright, young main-sequence stars in each of these LMC fields (different values of τ_F).

Our analysis indicates that, while other sorts of SFRs do not lead to acceptable results, the burst hypothesis yields number ratios of stars in selected areas of the CMDs that agree with the observed starcounts if the correct type of stellar models and a suitable value of the distance modulus are adopted. Using overshoot models and assuming a true distance modulus of 18.4, our analyses of the NGC 1783, NGC 1866, and NGC 2155 fields suggest that τ_B is very similar in each. Thus, a burst in the star formation *commenced* at nearly the same time in each of the fields we have studied. In addition to this, it seems plausible that the classical Salpeter law for the IMF is holding for the field stars of LMC. In fact, no need has been found for a different slope.

It is worth emphasizing that our primary conclusion, that is, the possibility of a single burst of star formation, depends on the modulus of $(m-M)_0 = 18.4$. If $(m-M)_0 = 18.6$ is adopted, then there is no longer strong evidence for a single burst throughout the LMC. Remarkably, this indirect estimate of the distance modulus is consistent with the recent determination by Panagia et al. (1991) based on the circumstellar ring observed by HST around the supernova 1987A.

The value of τ_B we find agrees with the (3–4) $\times$ 10^9 yr quoted by Butcher (1977). Consequently, we confirm Butcher's findings that a significant fraction of the field stars in the LMC formed well after the initial formation of the galaxy itself. Our results imply that the LMC was quiescent for about 70% of its lifetime as suggested from Butcher's quantitative results. To be sure, there is ample evidence that *some* star formation occurred prior to the "burst" in the LMC SFR. For example, the presence of a small number of old clusters (Stryker et al. 1984; Walker 1985, 1989, 1990; Mateo, Hodge, & Schommer 1986), RR Lyrae field stars (Graham 1977), and low-mass long-period variables (Bessell, Freeman, & Wood 1986) are all indicative of a true old (age $\geq 10 \times 10^9$ yr) population of stars. However, our findings indicate that the mean star formation rate in the LMC has subsequently been as much as 10 times higher since the "burst" began and that this sort of enhanced star formation rate was sustained up to at least 1 Gyr ago even in the outer parts of the LMC. In the central regions of the LMC, star formation is clearly continuing to the present day. The age distribution of LMC clusters seems to be similar since the great majority of all well-studied red clusters have ages less than about 3×10^9 yr (Da Costa 1991; Olszewski et al. 1991). The apparent similarity of the age distribution of the oldest stars in a number of widely separated LMC fields further suggests that whatever event triggered this "burst" in the SFR did so globally and rather suddenly. It is tempting to attribute the LMC starburst trigger to some sort of dynamical interaction between the Galaxy, LMC, and SMC (Murai & Fujimoto 1980). However, if the LMC and SMC have always been close together (and this is by no means certain), why is the SMC field and star cluster age distribution apparently skewed toward

much older ages compared to the LMC (Hardy & Durand 1984)? Did the SMC not experience the same perturbation that enhanced the SFR in the LMC? The existence of noninteracting, but active, dwarf galaxies (e.g., NGC 4449; Bothun 1986) suggests that a tidal trigger may not be the only way to initiate a burst of star formation in a dwarf galaxy. What sort of internal mechanism can initiate such a global star formation "burst" such as the one that seems to have occurred in the LMC? Such a radically variable SFR should leave indelible imprints on the chemical enrichment history of the LMC—what are these imprints and do they agree with observational constraints? The striking discontinuity in the age-abundance relation for the LMC clusters (Olszewski et al. 1991) may be part of the signature of the complex chemical evolution that accompanied the star formation burst we identify in our analysis of the LMC field stars. Understanding the LMC field star age distribution and how and why it differs from the SMC will clearly not only ultimately teach us much about these nearby systems, but about the evolution of other dwarf galaxies as well.

We thank Robert Schommer, Edward Olszewski, and the late Marc Aaronson for the use of their NGC 2155 data in this study. DoPHOT was developed by Paul Schechter under grant AST 83-18504 from the US National Science Foundation, and we thank him for his permission to use the code for this work. This work was supported by the Italian Ministry of University, Scientific Research and Technology (MURST) and the Italian Space Agency (ASI). Partial support was also provided by NASA through grant HF-1007.01-90A awarded by the Space Telescope Science Institute which is operated by the Association of Universities for Research in Astronomy, Inc., for NASA under contract NAS5-26555.

REFERENCES

Aparicio, A., Bertelli, G., Chiosi, C., & Garcia-Pelayo, J. M. 1990, A&A, 240, 262
Bertelli, G., Betto, F., Bressan, A., Chiosi, C., Nasi, E., & Vallenari, A. 1990, A&AS, 85, 845
Bertelli, G., Bressan, A., & Chiosi, C. 1985, A&A, 150, 33
Bertelli, G., Bressan, A., Chiosi, C., & Angerer, K. 1986a, A&AS, 66, 191
———. 1986b, in The Age of Star Clusters, ed. F. Caputo, Mem. Soc. Astron. Ital., 57, 427
Bessell, M. S., Freeman, K. C., & Wood, P. R. 1986, ApJ, 310, 710
Bothun, G. D. 1986, AJ, 91, 507
Bressan, A., Bertelli, G., & Chiosi, C. 1981, A&A, 102, 25
———. 1986, Mem. Soc. Astron. Ital., 57, 427
Butcher, H. 1977, ApJ, 216, 327
Castellani, V., Chieffi, A., & Straniero, F. A. 1989, ApJS, 74, 463
Chiosi, C., Bertelli, G., & Bressan, A. 1988, A&A, 196, 84
Chiosi, C., Bertelli, G., Meylan, G., & Ortolani, S. 1989, A&A, 219, 167
Da Costa, G. S. 1991, in The Magellanic Clouds, ed. R. Haynes & D. Milne (Dordrecht: Reidel), 183
Elson, R. A. W. 1991, ApJS, 76, 185
Elson, R. A. W., Fall, S. M., & Freeman, K. C. 1987, ApJ, 323, 54
Fagotto, F. 1990, Ph.D. thesis, Univ. Padova
Fischer, P., Welch, D. L., Côté, P. Mateo, M., & Madore, B. F. 1991, AJ, submitted
Frogel, J. A., & Blanco, V. M. 1983, ApJ, 274, L57
Graham, J. A. 1977, PASP, 89, 425
———. 1981, PASP, 93, 29
———. 1982, PASP, 94, 244
Green, E. M., Bessel, M. S., Demarque, P., King, S. R., & Peters, W. L. 1987, in The Revised Yale Isochrones and Luminosity Functions (New Haven: Yale Univ. Observatory)
Hardy, E., Buonanno, R., Corsi, C. E., Janes, K. A., & Schommer, R. A. 1984, ApJ, 278, 592
Hardy, E., & Durand, D. 1984, ApJ, 279, 567
Hodge, P. W. 1973, AJ, 78, 807
———. 1983, ApJ, 264, 470
Lattanzio, J. C. 1986, ApJ, 311, 708
———. 1987a, in Late Stages of Stellar Evolution, ed. S. Kwok & S. R. Pottash (Dordrecht: Reidel), 235
Lattanzio, J. C. 1987b, ApJ, 313, L15
———. 1991, ApJS, 76, 215
Maeder, A. 1974, A&A, 32, 177
Mateo, M. 1987a, Ph.D. thesis, Univ. Washington
———. 1987b, ApJ, 323, L41
———. 1988a, in The Harlow Shaply Symposium on Globular Cluster Systems in Galaxies, ed. J. E. Grindlay & G. D. Phillip (Dordrecht: Reidel), 557
———. 1988b, ApJ, 331, 261
Mateo, M., Hodge, P., & Schommer, R. 1986, ApJ, 311, 113
Mateo, M., Olszewski, E. W., & Madore, B. F. 1990, ApJ, 353, L11
Mateo, M., & Schechter, P. 1989, in The First ESO Data Analysis Workshop, ed. P. J. Grosbøl, F. Murtagh, & R. H. Warmels (ESO: Garching), 69
Murai, T., & Fujimoto, M. 1980, PASJ, 32, 581
Nail, V. M., & Shapley, H. 1953, Proc. Natl. Acad. Sci., 39, 358
Olszewski, E. W., Schommer, R. A., & Aaronson, M. 1987, AJ, 93, 565
Olszewski, E. W., Schommer, R. A., Suntzeff, N. B., & Harris, H C. 1991, AJ, 101, 515
Panagia, N., Gilmozzi, R., Macchetto, F., Adorf, H. M., & Kirshner, R. P. 1991, ApJ, 380, L23
Ratnatunga, K. U., & Bahcall, J. N. 1985, ApJS, 59, 63
Salpeter, E. E. 1955, ApJ, 121, 161
Stetson, P. B., & Harris, W. E. 1988, AJ, 96, 909
Stryker, L. L. 1984, in Structure and Evolution of the Magellanic Clouds, ed. S. van den Bergh & K. S. de Boer (Dordrecht: Reidel), 79
Stryker, L. L., Nemec, J. M., Hesser, J. E., & McClure, R. D. 1984, in Structure and Evolution of the Magellanic Clouds, ed. S. van den Bergh & K. S. de Boer (Dordrecht: Reidel), 43
Tifft, W., & Snell, C. 1971, MNRAS, 151, 365
Vallenari, A., Chiosi, C., Bertelli, G., Meylan, G., & Ortolani, S. 1991a, A&AS, 87, 517
———. 1991b, AJ, submitted
van den Bergh, S. 1984, A&AS, 46, 79
Walker, A. R. 1985, MNRAS, 212, 343
———. 1989, AJ, 98, 2086
———. 1990, AJ, 100, 1532